RSC Advances

ROYAL SOCIETY OF CHEMISTRY

www.rsc.org/advances

Thermal Decomposition Kinetics of Light Polycyclic Aromatic Hydrocarbons as Surrogate Biomass Tar

Chao Gai[a], Yuping Dong[b,*], Shuai Yang[b], Zhaoling Zhang[c], Jingcui Liang[c], Jingdong Li[c]

[a] Research Center for Eco-Environmental Sciences, Chinese Academy of Sciences, 18 Shuangqing Road, Beijing 100085, PR China.

[b] School of Mechanical Engineering, Shandong University, Jinan 250061, PR China.

[c] Shandong Baichuan Tongchuang Energy Company Ltd., Jinan 250101, PR China.

Corresponding author

Yuping Dong, dongyp@sdu.edu.cn, Tel: +86 (531) 88392199

Address: 17923 Jingshi Road, Jinan 250061, PR China.

Abstract

Thermal decomposition of the two light polycyclic aromatic hydrocarbons (PAHs), naphthalene and anthracene as tar model compounds was investigated on a lab-scale fluidized bed reactor. Pyrolysis kinetics for the four main gaseous products, including hydrogen, methane, ethylene and propane were evaluated. Experimental results indicated that naphthalene with two fused benzene rings was easier to be decomposed than that of anthracene with three fused benzene rings. The apparent activation energies of hydrogen, methane, ethylene and propane for naphthalene were 33.9 kJ/mol, 51.7 kJ/mol, 49.1 kJ/mol and 27.2 kJ/mol, respectively. The apparent activation energies of hydrogen, methane, ethylene and propane for anthracene were 148.0 kJ/mol, 52.2 kJ/mol, 86.4 kJ/mol and 63.8 kJ/mol, respectively. The most probable reaction mechanisms describing the evolution profiles of individual gas components from the pyrolysis of the two PAHs were three-dimensional diffusion for hydrogen, methane, and propane, as well as chemical reaction for ethylene.

Key words

Pyrolysis; Naphthalene; Anthracene; Soot; Kinetic; Activation energy

1. Introduction

Increasing in the greenhouse gas (GHG) levels worldwide from anthropogenic activities like the combustion of fossil fuels for power/heat generation is one of the major contributors to climate change. It necessitates a turning to renewable energy sources in terms of wind, solar photovoltaic, and biomass.[1,2] As the carbon-neutral renewable sources, biomass can be converted to renewable biofuels with various conversion approaches.[3,4] Gasification can convert precursory biomass into syngas, which is viewed as one of the most promising ways to utilize abundant biomass. However, tar is an inevitable byproduct during the gasification process.[5-6] It will render wasting of energy, reducing gas calorific value and gasification efficiency, as well as affecting the stable and safe operation of the gasification equipments. Consequently, the proficient removal or conversion of biomass tar has become one of the key issues in large-scale biomass gasification processes. Tars can be removed by physical and thermal cracking (non-catalytic or catalytic) measures. Thermal cracking is a technically and economically interesting approach for gas cleaning, which has received increasing attention.[7-8] To detailedly investigate the mechanism of thermal cracking of biomass tar, it is essential to simplify the reaction process by applying suitable surrogate biomass tar and precise lab-scale reactor.

The composition of tar is extremely complex in terms of phenolic, alkylated aromatic and polycyclic aromatic hydrocarbons (PAHs).[9-11] To overcome the complexity of tar, researchers have conducted extensive studies on several tar model compounds in terms of phenolic compounds (e.g., phenol, cresols) and alkylated

aromatic compounds (e.g., toluene, xylene, styrene).[12] Previous studies showed that the phenolic and aromatic compounds are easy to be degraded with increased temperatures. Gil et al. [13] investigated the steam gasification of wood, it was reported a 50% reduction of toluene when the temperature was raised from 700 to 900 ^{o}C. Brage et al. [14] observed an almost complete reduction of phenol with the increment of temperature from 700 to 900 ^{o}C. However, the light PAH compounds such as naphthalene and anthracene, are hard to be thermally cracked than phenolic and aromatic tar compounds.[15] In addition, various gasification studies [16-17] indicate that PAHs are the major components at relatively high temperatures (700-900 ^{o}C). According to Han et al.,[12] the relative contents of naphthalene and anthracene in tar are usually above 9% and 3%. Coll et al. [18] investigated the reactivity of five tar model compounds during the gasification process, and it was observed that naphthalene was the most suitable compound for use as a tar model compound during the biomass gasification. Besides, soot formation during the catalytic cracking of tar should be paid special attention because the formed soot may deposit on the active sites of the inner pore surface of the catalyst, leading to the deactivation of the catalyst and decreasing the tar removal efficiency. According to Tenser et al.,[19] the sooting tendencies for naphthalene and anthracene were both far higher than other components (e.g., aromatics, aliphatics) in biomass tar. Therefore, we used naphthalene and anthracene as the tar model compounds in this work.

Different heating strategies have been applied to study the decomposition behavior of tar model compounds. To date, thermal cracking kinetics of tar model

compounds has been carried out on different heating reactors such as thermo-gravimetric analyzer, [20-21], fixed-bed reactor, [22] continuous flow packed bed reactor [23] and tubular flow reactor [24]. In this study, the pyrolysis behavior of the tar model compounds was investigated on a novel lab-scale fluidized bed reactor (FBR). [25-26] The facility can strengthen the heat transfer and mass transfer of gas-solid reaction via the fluidized bed. Additionally, it can send the materials into the reactor instantaneously when the temperature within the reactor has been heated to a desired level, which can minimize the inhibition of the diffusion.[27] In this study, the thermal decomposition behavior of the two light PAH compounds, naphthalene and anthracene, as the model compounds of biomass tar were studied on the FBR. The product distribution and evolution of non-condensed gas products as a function of temperature were investigated in FBR. Pyrolysis kinetics of the two light PAHs were further determined. The most probable reaction models for major gaseous products during the decomposition of the two tar model compounds were further proposed.

2 Experimental section

2.1 Materials

Two light polycyclic aromatic hydrocarbons (PAHs), naphthalene and anthracene were chosen as the model compounds of biomass tar. They were purchased from Sigma-Aldrich without further purification, and their properties were illustrated in Table 1.

2.2 Reactor system

Pyrolysis experiments of naphthalene and anthracene were conducted in a

lab-scale fluidized bed reaction system, which is shown in Fig.1. It is mainly composed of a quartz fluidized bed reactor, a sample-feeding device and process controlling system. The lab-scale quartz fluidized bed reactor is the key part of the FBR. The diameter of the reactor is 290 mm, and the height is 373 mm. The reaction zone's inner diameter is 20 mm and the height is 42 mm, which is similar to that of the thermogravimetric analyzer. The reaction zone has two uniform plates with evenly distributed holes for gas distribution. The sample is sent to the reaction zone via the sample-feeding device, which is driven by an electromagnetic valve that can inject the sample into the reactor within 0.1 s by the pulse. The pulsed gas originates from a compressed gas stream at 0.2 MPa via a tube with an inner diameter of 3 mm. The process mass spectrometer can measure the relative content of produced gas online. The temperatures of the electric furnace and reactor are controlled by computer. Besides, the computer monitors the flow rate of the fluidizing gas, the pressures at the inlet and outlet of the reactor, actions of sample-feeding system and the output data from the process mass spectrometer.

2.3 Experimental procedure

In this study, quartz sand with a mesh range of 65 to 80 was selected as the fluidizing medium. At the start of each test, 3.0 g of quartz sand was loaded into the fluidized bed reactor. 10±0.1 mg solid sample was placed at the end of the inlet pipe of the sample-feeding system. The gas tightness of the whole reaction system was inspected. Then the fluidizing gas, Ar (99.99% purity), was fed to the reactor to fluidize the materials in the reactor. Afterwards, the reactor was heated to preset

temperatures. Then the pulse valve of the sample-feeding system was switched on to inject the sample into the reaction zone, which initiated the pyrolysis reaction.

According to Jess [28] and Fuentes-Cano et al.,[29] the thermal cracking of polycyclic aromatic hydrocarbons (PAHs) resulted in hydrocarbons with smaller carbon numbers, and intermediates such as toluene, indene or indane were formed to only a limited extent. In this study, the major non-condensable gas derived from pyrolysis of PAHs, including hydrogen (H_2) as well as light hydrocarbons (C1-C3) such as methane (CH_4), ethylene (C_2H_4) and propane (C_3H_8) were analyzed. Olefins (>C4) was negligible in this work. To determine the yield (in mass against precursor feedstock) of each permanent gas, the gaseous products were all sampled in the entire reaction time and then analyzed by a Micro-GC 3000 (gas chromatography) equipped with a TCD (thermal conductivity detector) and two columns (5A and GDX-104). The oven temperature was 60 ^{o}C, and the temperature for the TCD was 150 ^{o}C. The carrier gas was argon, and a standard gas mixture was applied to calibrate the yield of non-condensable gas. The sum of the individual gas yield was regarded as the total gas yield. The inner surface of the reactor was observed to be coated with a layer of soot during the tests, which is formed during the pyrolysis of larger PAHs.[30] It is determined by weighing the fluidized bed reactor before and after the experiments.

The decomposition temperatures of naphthalene and anthracene were ranged from 700 ºC to 900 ºC with 50 ºC intervals. In this study, several preliminary tests were conducted to determine the minimum fluidization rate and optimum flow rate of the carrier gas. It was observed that the minimum fluidization rate for the quartz sand

was 220 mL/min. Furthermore, increasing the gas flow rate from 220 to 500 mL/min gradually increased the total gas yield, while a small variation of the total gas yield was observed when the flow rate was higher than 500 mL/min. Consequently, to ensure the complete fluidization of the quartz sand, the flow rate of the carrier gas was maintained at the level of 500 mL/min in this study.

2.4 Kinetic approaches

Pyrolysis of tar model compound is a complex physical and chemical process, such as mass transfer, polymerization/depolymerization. The homogeneous reaction of the thermal decomposition of the two PAHs under different reaction temperatures is described as:

$$dx/dt = k(T) \times f(x) \tag{1}$$

where T is the reaction temperature, t is the reaction time, f(x) is the differential reaction model, x is the conversion fraction of each gas composition and it can be calculated through:

$$x = \frac{\int_{t_0}^{t} C_i \times C dt}{\int_{t_0}^{t_e} C_i \times C dt} \times 100\% \tag{2}$$

where t_0 is the start time of pyrolysis reaction, t_e is the end time of pyrolysis reaction, C is the rate of volume for all gas components, C_i is the rate of the volume fraction for the gas composition i. It should be noted that the conversion fraction of 100% corresponds to the highest gas yield at the end of the reaction, and the time spent for increasing conversion fraction from 0 to 100% is defined as the reaction finishing time.

In Eq.(1), k(T) is the rate constant of reaction and it is determined by Arrhenius equation:[6,31]

$$k(T) = A\exp(-E_a/RT) \tag{3}$$

where E_a is the apparent activation energy, A is the pre-exponential factor, T is the thermodynamic temperature, R is the gas constant, 8.314 $J\cdot(mol\cdot K)^{-1}$.

Take the logarithm of both sides of Eq. (1) and Eq. (3) results in the Eq. (4) and Eq. (5), respectively.

$$\ln\frac{dx}{dt} = \ln k(T) + \ln f(x) \tag{4}$$

$$\ln k(T) = \ln A - \frac{E_a}{RT} \tag{5}$$

Substituting Eq.(5) into Eq.(4), which is expressed as:

$$\ln\frac{dx}{dt} = -\frac{E_a}{RT} + \ln A + \ln f(x) \tag{6}$$

At different temperatures, the points of ln (dx/dt) versus 1/T can be fitted to a straight line, and the apparent activation energy can be deduced from the slope which corresponds to $-E_a/R$.

Substituting Eq.(3) into Eq.(1), which is expressed as:

$$dx/dt = A\exp(-E/RT)\times f(x) \tag{7}$$

Carrying out the integration of the both sides of Eq. (7) in reaction time (t) under a certain temperature (T), and it can be further integrated into Eq. (8),

$$G(X) = \int_0^x dx/f(x) = k(T)\times t \tag{8}$$

where G(x) is the integral reaction model. If the curve of G(x) versus t is linear, then k(T) is the slope, and G(x) with the highest linear correlation coefficient is the most

probable reaction mechanism. Afterwards, a number of curves of x versus t under different temperatures could be obtained, then we can get a set of values of k(T). Based on Eq.(5), the plots between lnk(T) versus 1/T can generate a straight line with the slope of $-E_a/R$ to determine the apparent activation energy again. Then the proposed kinetic model for pyrolysis of the two PAHs can be determined based on the closeness of the value of apparent activation energies.

3 Results and discussion

3.1 Product yields

In the pyrolysis step, the two light PAHs undergoes fast decomposition to products in different phases. Figure 2 illustrated the product distribution during the pyrolysis of naphthalene and anthracene in the FBR at temperatures from 700 to 900 ^{o}C. Mass balance analyses indicate that a substantial fraction, 70-90 wt.% of the two PAHs were cracked into non-condensed gas, while 2-10 wt.% of the two PAHs were converted to soot. The gas yields for the thermal cracking of the two PAHs are much higher than that of in the fixed bed reactor, accompanied with a lower amount of solid carbonaceous residue (soot) formed during the pyrolysis process. This provides evidence of higher heating rate and more efficient mass-transfer in the FBR.

Under identical temperature, the soot yield of naphthalene was a bit higher than that of anthracene. Tesner et al. [19] developed sooting tendency factors ($N_0 / N_{0(CH_4)}$, N_o refers to the number of soot particles in 1 g of soot) as a means to compare the soot formation during pyrolysis of different PAHs. The reported sooting tendency for naphthalene (110) was higher than that of anthracene (102). This provides quantitative

evidence suggesting that more soot will be formed during the pyrolysis of naphthalene than that of anthracene, which is verified by the mass balance analyses in this work. Additionally, a rapid increase of soot yield was observed at 800 ^{o}C for naphthalene (from 4.4 to 8.7%) and at 850 ^{o}C for anthracene (from 3.2 to 7.9%). It implies that a transition temperature for soot formation of naphthalene is 800 ^{o}C while the polymerization of anthracene occurs at a higher temperature (850 ^{o}C).

The mass balance was not closed. Around 1-17 wt.% of naphthalene and 6-25 wt.% of anthracene could not be quantitatively determined (Fig. 2). Some soot precursor species derived from the thermal cracking of PAHs may account for the incomplete balance. Besides, some PAHs may be left from the reactor without reaction because naphthalene and anthracene are quite volatile at higher temperatures.[32] A certain amount of PAHs may also be adsorbed on the soot. Sánchez et al [33] reported that the amount of PAHs adsorbed on the soot during the pyrolysis of PAHs was much larger than that adsorbed on the reactor wall or retained in the outlet gas. As shown in Fig.2, increasing temperature promoted soot formation and inhibited undetected compounds. Therefore, it could be speculated that some PAHs adsorbed on the soot may be converted to soot with the increased temperature. Follow-up experiments should take into account both the PAHs adsorbed on the soot and reactor walls.

The gas produced during the cracking process accounted for approximately 70-90 wt.% of the two PAHs, and the evolutions of gas composition as a function of cracking temperature were illustrated in Fig.3. The gaseous products produced from the two PAHs were predominantly ethylene and propane with trace amounts of

methane and hydrogen. The yields of various gaseous products have different variations as a function of temperature. As shown in Fig.3, the yield of propane for the two PAHs both underwent a process of a fall after a rise. It suggests that a further increase of temperature promotes the decomposition of propane to form methyl and ethyl radicals.[34] The methyl radical is the main source for methane production, which is very active and can react with hydrogen or ethylene to form methane.[35] Therefore, the continuously increased methane yield shown in Fig.3 suggest that the reaction between ethylene and methyl radicals from propane to form methane is favored during the decomposition of the two PAHs at higher temperatures. It accounts for the decrease of ethylene and propane at higher temperatures. Besides, ethylene is an important precursor of PAHs and soot, which can undergo simultaneous dehydrogenation at the gas phase to generate PAHs and soot via the hydrogen abstraction acetylene addition (HACA) route.[36-37] In this work, the decreased yield of ethylene as a functional of temperature (Fig.3) is consistent with the increased soot (Fig.2) for the two PAHs, implying that more ethylene produced from the decomposition of the two PAHs are converted to soot at higher temperatures. This observation is in accordance with the findings by Sánchez et al.,[38] who investigated the pyrolysis of ethylene and observed that the soot formation was enhanced for ethylene pyrolysis with increased temperature.

The increment of the cracking temperature from 700 to 900 ^{o}C caused a gradual increase of hydrogen for the two PAHs. The decomposition of PAH in tars is usually explained by a dehydrogenating polymerization process accompanied with an

aromatization growth,[39] notwithstanding a comprehensive knowledge of this process is currently not available due to the complexity of reactions that occur during the biomass pyrolysis. During the cracking of PAHs, hydrogen is mostly generated from the dehydrogenation process ($pC_xH_y \rightarrow qC_nH_m + rH_2$; where n<x and m<y), which reflects the extent of the tar polymerization reaction. In this work, the hydrogen yield derived from the two PAHs both increased gradually with the increased temperature, although hydrogen accounted for a smaller fraction of the total gas yield. Similarly to that described by Anis et al.,[40] an increase of hydrogen yield with increased temperature during the pyrolysis of toluene was also observed. This provides evidence implying that the polymerization of naphthalene and anthracene occurs during the thermal decomposition process, and it is promoted by the increased temperature. Huang et al. [41] employed a density functional theory to study the decomposition pathway of aromatic hydrocarbons during the coal pyrolysis process. It was reported that the hydrogen atoms play an important role in the initiation of benzene decomposition. In the tar pyrolysis, the role of hydrogen is more like a hydrogen transfer intermediate, which contributes to the decomposition of heavy tar compounds into lighter tar molecules and polymerizes smaller tar species into larger tar compositions.[28]

3.2 Gas evolution profiles of pyrolysis of naphthalene and anthracene

During the pyrolysis of naphthalene and anthracene in FBR, the release characteristics of individual gas components, including H_2, CH_4, C_2H_4 and C_3H_8, at the preset temperatures of 700-900 ^oC were shown in Fig.4 and Fig.5, respectively. As

expected, for the same non-condensed gas, the reaction finishing time was greatly decreased with increasing the cracking temperatures. This is a kinetic effect, where a higher temperature promotes the reaction rate of the thermal cracking of these tar compounds to generate gaseous products. Additionally, at a certain cracking temperature, it can be seen that the reaction rate at the initial stage is the highest for each individual gas. This is because the tar model compounds were sent into the reaction zone at the required reaction temperature instead of the room temperature.

Some differences could be observed for the pyrolysis process of the two model compounds in the FBR. At higher temperatures, the reaction finishing time for each individual gas from the same model compound has not too many differences. For example, at the temperature of 900 ^{o}C, the reaction finishing time of four gaseous products from pyrolysis of naphthalene was all around 15-20s, which was lower than that of anthracene (approximately 40s for each gas component). The chemical structures for the two tar model compounds are different, although they both belong to PAHs. This provides evidence implying that during the thermal cracking of PAHs, it takes more time to break down three fused benzene rings into small molecules than that of compounds with two fused benzene rings. However, at lower temperatures, the reaction finishing time for different gas components is different. For the pyrolysis of naphthalene, the reaction finishing time of CH_4 and C_2H_4 was longer than that of H_2 and C_3H_8, while the reaction finishing time of H_2 and C_2H_4 was longer than that of CH_4 and C_3H_8 for anthracene. It indicates that during the pyrolysis process of naphthalene and anthracene, the releasing pathways of different gas components

should be different, especially for C_2H_4, which will be analyzed in next section.

3.3 Pyrolysis kinetics of naphthalene and anthracene

Apparent activation energies for the main gas components during the pyrolysis of naphthalene and anthracene in the FBR were first calculated and shown in Table S1. According to the literature,[42-43] most common nineteen reaction models for thermal cracking of biomass tar were applied in this study to fit the evolution profiles of individual gas component during the pyrolysis of naphthalene and anthracene, which is available in the supplementary data (Table S2). Among the nineteen models, five reaction models with best linearity were selected and plotted (Fig.S1 and Fig.S2). The corresponding apparent activation energies and fitting accuracy calculated were illustrated in Table S3 and Table S4. Among the five probable reaction models selected, the most probable reaction model describing the kinetic process was determined based on the closest values of apparent activation energy deduced from Table S1, Table S3 and Table S4. Table 2 illustrated the proposed reaction models and kinetic parameters for individual gas component during the thermal cracking of the two PAHs in FBR.

A reaction with lower apparent activation energy requires less energy to break down the chemical bonds between atoms and hence the reaction rate is faster, accompanied with a shorter residence time. During the pyrolysis of naphthalene, the apparent activation energies of CH_4 (51.7 kJ/mol) and C_2H_4 (49.1 kJ/mol) were higher than that of H_2 (33.9 kJ/mol) and C_3H_8 (27.2 kJ/mol). In terms of the pyrolysis of anthracene, the apparent activation energies of H_2 (148.0 kJ/mol) and C_2H_4 (86.4

kJ/mol) were higher than that of CH_4 (52.2 kJ/mol) and C_3H_8 (63.8 kJ/mol). The value of apparent activation energy for individual gas components were consistent with the corresponding reaction finishing time observed in Fig.4 and Fig.5. This provides evidence suggesting that compared to the thermal decomposition of anthracene, dehydrogenating process is more favored for naphthalene. Apparent activation energies of the thermal decomposition of other tar model compounds in the literature were reported in the range of 63-72 kJ/mol for naphthalene,[29] 150-156 kJ/mol for benzene,[44] and 197-281 kJ/mol for toluene.[45] It is difficult, however, to make direct comparisons between the activation energies reported in the literature and those calculated in this work, as tar precursor species, reactor scales and operation conditions all influence the thermal decomposition pathway of the tar model compounds.

In this work for the same gas component, the apparent activation energy of the pyrolysis of naphthalene was lower than that of anthracene. It further verifies that for the two tar model compounds, the thermal cracking of naphthalene with two-membered rings is easier than that of anthracene with three-membered rings. For the reaction of PAHs with atmospheric oxidants (e.g. OH), Keyte et al.[46] reported that 3-ring PAHs being more stable than 2-ring structures at higher temperatures. Brubaker et al.[47] studied the kinetics of the 4-ring fluoranthene and concluded that it would form a more stable OH-adduct than 2- or 3-ring structures. Liu et al.[48] also observed that five-membered ring was easier to decompose than the six-membered ring. Taking into account the differences in the experimental facilities and reaction conditions, the

result in this work coincides with the previous literature.

As shown in Table 2, the reaction mechanism of three-dimensional diffusion could describe most individual gas components during the pyrolysis of the two PAHs in FBR, including hydrogen, methane, and propane. The production of hydrogen from naphthalene and anthracene followed the three-dimension diffusion (A-J) and three-dimension diffusion (Jander), respectively. The generation of propane from naphthalene, three-dimension diffusion (Jander) was also slightly different from that of anthracene three-dimension diffusion (G-B). As shown in Fig.3, the critical temperature of the rapid increase in hydrogen concentration for naphthalene (800 ^{o}C) was different from that of anthracene (850 ^{o}C). The turning point of the propane yield produced from the decomposition of naphthalene and anthracene as a function of temperature was 800 and 850 ^{o}C, respectively. It implies that tar polymerization reactions and decomposition of propane during the pyrolysis of naphthalene and anthracene are favored by different temperatures. Therefore, the hydrogen and propane generated from naphthalene follow different reaction models with that of anthracene.

The releasing of ethylene for the two tar model compounds was described by the mechanism of chemical reaction with different reaction orders (n=2 for naphthalene and n=1 for anthracene), which is totally different from other three gaseous products. It is likely during the thermal decomposition of the two PAHs, the reaction pathway of ethylene is greatly different to other gaseous products. During the decomposition of the two PAHs, the ethylene may be aromatized via a reversible Diels-Alder reaction,

which occurs between a conjugated diene and a substituted alkene to generate a substituted cyclohexene system. Literature indicated that the thermal decomposition pathways of PAHs are dependent on the type of PAH radical sites in terms of zigzag, free-edge, and armchair.[48-49] To provide a theoretical investigation of decomposition pathways of PAHs, a detailed density functional theory is recommended for further study.

It should be noted that in this study, two simple tar model compounds were used. Therefore, the thermal decomposition behavior and kinetic analysis of the two PAHs provide realistic results (shown in Fig.6). As we know that in real situation, biomass tar is not only a mixture of the two PAHs applied, but it is a complex mixture of various organic compounds. The components of tars can be divided into different classes by various aspects in terms of molecular weight, formation temperature and the number of rings of tar compounds. [50-51] The interactions among the reaction intermediates produced from those tar components will greatly affect the reaction pathway of the thermal cracking of the PAHs.[12] All types of the chemical interactions at the molecular level are still unknown. Furthermore, there are some differences between the laboratory-scale reactor applied in this study and pilot-scale reactor. For example, laboratory-scale reactor can provide very high heat and mass transfer rates that can rarely be achieved using industrial reactors. The microscale studies gave a little thought to the secondary cracking reactions due to the short reaction time, which are fairly occurring in industrial reactors. Consequently, a detailed investigation of thermal decomposition characteristics of real tar in pilot scale may provide new

insights into the reaction mechanisms of tar reduction, which is recommended for future study.

4 Conclusions

Thermal decomposition kinetics of the two light PAHs as tar model compounds, naphthalene and anthracene were studied on a novel lab-scale fluidized bed reactor. The results revealed that naphthalene with two-membered rings was easier to decompose than anthracene with three-membered rings during the thermal cracking of biomass tar. More soot was formed for naphthalene rather than anthracene under identical decompositon temperature. The main gaseous products generated from the two PAHs were ethylene and propane with little methane and hydrogen. Dehydrogenating polymerization plays a key role in the thermal decomposition of the two PAHs and soot formation. The results imply that for the thermal decomposition of polycyclic aromatic hydrocarbons derived from biomass pyrolysis/gasification, the critical temperatures affecting the distribution of gaseous products as well as soot yield for naphthalene and anthracene are 800 ^{o}C and 850 ^{o}C, respectively. Besides, a detailed analysis of the chemical composition of the soot may help us investigate the reaction mechanism soot formation during the thermal cracking of PAHs, which is recommended for future study.

Acknowledgements

Financial support for this study that has been provided by National Key Foundation for Exploring Scientific Instrument (2011YQ120039) is gratefully acknowledged.

References

[1] D.M. Alonso, J.Q. Bond and J.A. Dumesic. Catalytic conversion of biomass to biofuels. *Green Chem*. 2010, **12**, 1493-1513.

[2] V.S. Sikarwar, M. Zhao, P. Clough, J. Yao, X. Zhong, M.Z. Memon, N. Shah, E.J. Anthony and P.S. Fennell. *Energy Environ. Sci.* 2016. DOI: 10.1039/C6EE00935B.

[3] A. Arregi, G. Lopez, M. Amutio, I. Barbarias, J. Bilbao and M. Olazar, *RSC Adv.*, 2016, **6**, 25975-25985.

[4] G. Gordillo, K. Annamalai and N. Carlin, *Renew. Energy*, 2009, **34**, 2789-2797.

[5] J.R. Kastner, S. Mani and A. Juneja, *Fuel Process. Technol.*, 2015, **130**, 31-37.

[6] G. Taralas and M.G. Kontominas, *J. Anal. Appl. Pyrol*., 2006, **76**, 109-116.

[7] Z. Abu EI-Rub, E.A. Bramer and G. Brem. Review of catalysts for tar elimination in biomass gasification processes. *Ind. Eng. Chem. Res.* 2004, **43**, 6911-6919

[8] D. Mei, V.M. Lebarbier, R. Rousseau, V.A. Glezakou, K.O. Albrecht, L. Kovarik, M. Flake and R.A. Dagle. *ACS Catal.* 2013, **3**, 1133-1143.

[9] R. Shu, Q. Zhang, Y. Xu, J. Long, L. Ma, T. Wang, P. Chen and Q. Wu, *RSC Adv.*, 2016, **6**, 5214-5222.

[10] A.M. Fraind and J.D. Tovar, *J. Phys. Chem. B.*, 2010, **114**, 3104-3116.

[11] H. Zhou, C. Wu, J.A. Onwudili, A. Meng, Y. Zhang and P.T. Williams, *RSC Adv.*, 2015, **5**, 11371-11377.

[12] J. Han and H. Kim, *Renew. Sust. Energ. Rev*., 2008, **12**, 397-416.

[13] J. Gil, J. Corella, M.P. Aznar and M.A. Caballero, *Biomass Bioenergy*, 1999, **17**,

389-403.

[14] C. Brage, Q. Yu, G. Chen and K. Sjöström, *Biomass Bioenergy*, 2000, **18**, 87-91.

[15] Q. Sun, S. Yu, F. Wang and J. Wang, *Fuel*, 2011, **90**, 1041-1048.

[16] C. Font Palma, *Appl. Energy*, 2013, **111**, 129-141.

[17] J. N. Putro, F. E. Soetaredjo, S. Y. Lin, Y. H. Ju and S. Ismadji, *RSC Adv.*, 2016, **6**, 46834-46852.

[18] R. Coll, J. Salvado, X. Farriol and D. Montane, *Fuel Process. Technol.*, 2001, **74**, 19-31.

[19] P.A. Tesner and S.V. Shurupov, *Combust. Sci. Technol*., 1997, **126**, 139-151.

[20] J.F. Saldarriaga, R. Aguado, A. Pablos, M. Amutio, M. Olazar and J. Bilbao, *Fuel*, 2015, **140**, 744-751.

[21] C. Gai, Y. Dong and T. Zhang, *Bioresour. Technol.*, 2013, **127**, 298-305.

[22] C. Brage, Q. Yu and K. Sjöström, *Fuel*, 1996, **75**, 213-219.

[23] S. Mani, J.R. Kastner and A. Juneja, *Fuel Process. Technol.*, 2013, **114**, 118-125.

[24] G. Taralas, M.G. Kontominas and X. Kakatsios, *Energy Fuel*, 2003, **17**: 329-337.

[25] F. Guo, Y. Dong, Z. Lv, P. Fan, S. Yang and L. Dong, *Energy Convers. Manage.*, 2016, **108**: 201-218.

[26] Y. Mao, Y. Dong, B. Wang, J. Chang, J. Yu, Y. Zhang, Y. Huo and C. Sun, *RSC Adv*., 2015, **5**, 82845-82852.

[27] J. Yu, C. Yao, X. Zeng, S. Geng, L. Dong, Y. Wang, S. Gao and G. Xu, *Chem. Eng. J*., 2011, **168**, 839-847.

[28] A. Jess, *Fuel*, 1996, **75**, 1441-1448.

[29] D. Fuentes-Cano, A. Gómez-Barea, S. Nilsson and P. Ollero, *Chem. Eng. J.*, 2013, **228**, 1223-1233.

[30] A.W. Palumbo, J.C. Sorli and A.W. Weime, *Appl. Energy*, 2015, **157**, 13-24.

[31] Chandrasekaran SR and Hopke PK. *Bioresour. Technol.*, 2012, **125**, 52-58.

[32] J. Aihara, *Phys. Chem. Chem. Phys.*, 1999, **1**, 3193-3197.

[33] N.E. Sánchez, A. Callejas, A. Millera, R. Bilbao and M.U. Alzueta, *Energy*, 2012, **43**, 30-36.

[34] Z.P. Tang, A.J. Li, Z.W. Zhang, X. Ma, W. Wang, J.M. Fang and R.C. Bai. *Ind. Eng. Chem. Res.* 2014, **53**, 17537-17546.

[35] K. Norinaga and O. Deutschmann. *Ind. Eng. Chem. Res.* 2007, **46**, 3547-3557.

[36] H. Wang and M. Frenhlach. *Combust. Flame* 1997, **110**, 173-221.

[37] D.B. Murphy, R.W. Carroll and J.E. Klonowski. *Carbon* 1997, **35**, 1819-1823.

[38] N.E. Sánchez, A. Callejas, Á.Millera, R. Bilbao and M.U. Alzueta. *Energy Fuel* 2012, **26**, 4823-4829.

[39] A.M. Mastral and M.S. Callén, *Environ. Sci. Technol.*, 2000, **34**, 3051-3057.

[40] S. Anis, Z.A. Zainal and M.Z.A. Bakar, *Bioresour. Technol.*, 2013, **136**, 117-125.

[41] X. Huang, D. Cheng, F. Chen and X. Zhan, *Int. J. Hydrogen Energ.*, 2012, **37**, 18040-18049.

[42] E. Ranzi, M. Corbetta, F. Manenti and S. Pierucci, *Chem. Eng. Sci.*, 2014, **110**, 2-12.

[43] M. Puig-Amavat, J.C. Bruno and A. Coronas, *Renew. Sust. Energ. Rev.*, 2010, **14**, 2841-2851.

[44] P.A. Simell, N.A.K. Hakala and H.E. Haario, *Ind. Eng. Chem. Res*., 1997, **36**, 42-51.

[45] S. Anis and Z.A. Zainal, *Bioresour. Technol*., 2014, **151**, 183-190.

[46] I.J. Keyte, R.M. Harrison and G. Lammel. *Chem. Sov. Rev*. 2013, **42**, 9333-9391.

[47] W.W. Brubaker and R.A. Hites, *J. Phys. Chem. A*. 1998, **102**, 915-921.

[48] P. Liu, H. Lin, Y. Yang, C. Shao, C. Gu and Z. Huang, *J. Phys. Chem. A*., 2014, **118**, 11337-11345.

[49] M. Celnik, A. Raj, R. West, R. Patterson and M. Kraft, *Combust. Flame*, 2008, **155**, 161-180.

[50] N.K. Kaisalo, M.L. Koskinen-Soivi, P.A. Simell and J. Lehtonen. *Fuel* 2015, **153**, 118-127.

[51] L.P.L.M. Rabou, R.W.R. Zwart, B.J. Vreugdenhil and L. Bos. *Energy Fuel* 2009, **23**, 6189-6198.

Tables and Figures Captions

Table 1. Polycyclic aromatic hydrocarbons applied in the pyrolysis experiment.

Table 2. Proposed reaction models and kinetic parameters for individual gas component during the thermal cracking of naphthalene and anthracene.

Fig.1. Scheme diagram of the lab-scale fluidized bed reaction system.

Fig.2. Product distribution for the thermal decmoposition of naphthalene and anthracene at different temperatures.

Fig.3. Evolution of gas composition during thermal cracking of naphthalene and anthracene as a function of temperature.

Fig.4. Evolution of conversion fractions versus reaction time at different temperatures for the thermal decmoposition of naphthalene.

Fig.5. Evolution of conversion fractions versus reaction time at different temperatures for the thermal decomposition of anthracene.

Fig.6. Thermal decomposition behavior and kinetic analysis of naphthalene and anthracene in lab-scale fluidized bed reaction system.

Table 1 Polycyclic aromatic hydrocarbons applied in the pyrolysis experiment.

Compound	CAS #	Formula	Structure	MW	Purity	Supplier
Naphthalene	91-20-3	$C_{10}H_8$	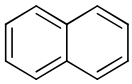	128	98%	Sigma-Aldrich
Anthracene	120-12-7	$C_{14}H_{10}$	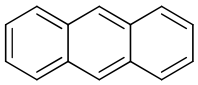	178	98%	Sigma-Aldrich

Table 2 Proposed reaction models and kinetic parameters for individual gas component during the thermal cracking of naphthalene and anthracene.

PAHs	Gas	E_a (kJ/mol)	Reaction mechanism	G(X)
Naphthalene	Hydrogen	33.9	Three-dimensional diffusion (A-J)	$[(1+x)1/3-1]^2$
	Methane	51.7	Three-dimensional diffusion (Jander)	$[1-(1-x)1/3]^2$
	Ethylene	49.1	Chemical reaction (n=2)	$(1-x)^{-1}-1$
	Propane	27.2	Three-dimensional diffusion (Jander)	$[1-(1-x)1/3]^2$
Anthracene	Hydrogen	148.0	Three-dimensional diffusion (Jander)	$[1-(1-x)1/3]^2$
	Methane	52.2	Three-dimensional diffusion (Jander)	$[1-(1-x)1/3]^2$
	Ethylene	86.4	Chemical reaction (n=1)	$-\ln(1-x)$
	Propane	63.8	Three-dimensional diffusion (G-B)	$1-2x/3-(1-x)^{2/3}$

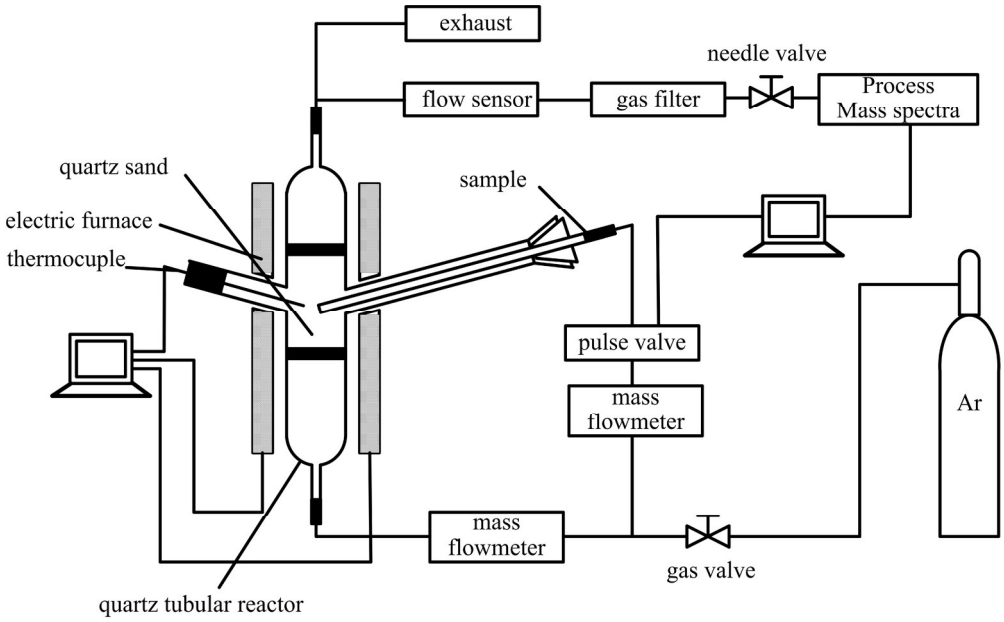

Figure 1 Scheme diagram of the lab-scale fluidized bed reaction system.

181x111mm (300 x 300 DPI)

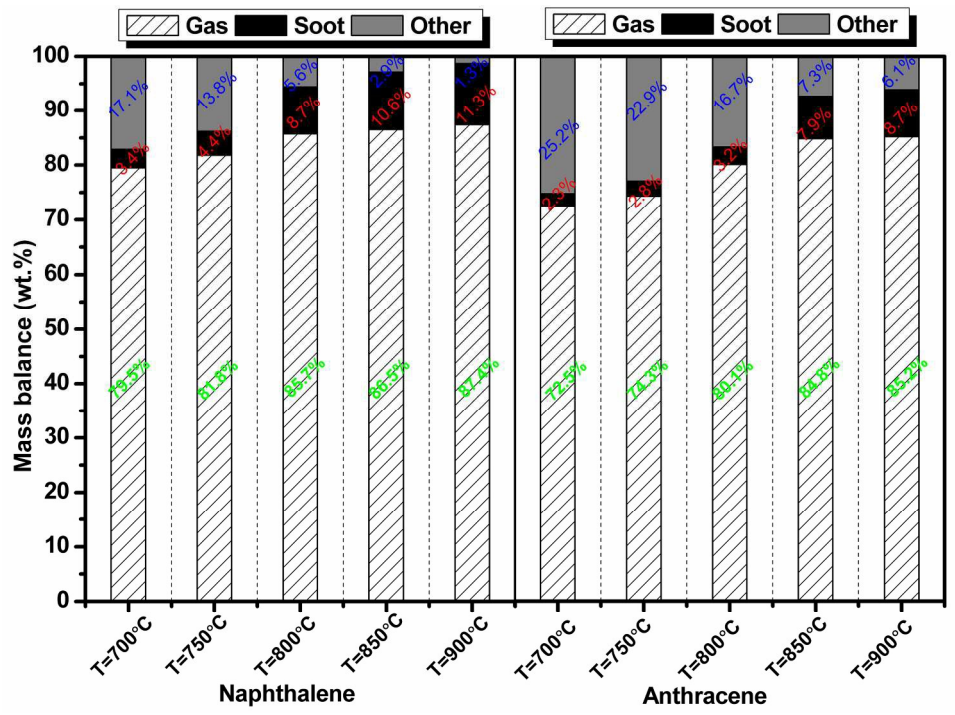

Figure 2 Product distribution for the thermal decmoposition of naphthalene and anthracene at different temperatures.

210x148mm (300 x 300 DPI)

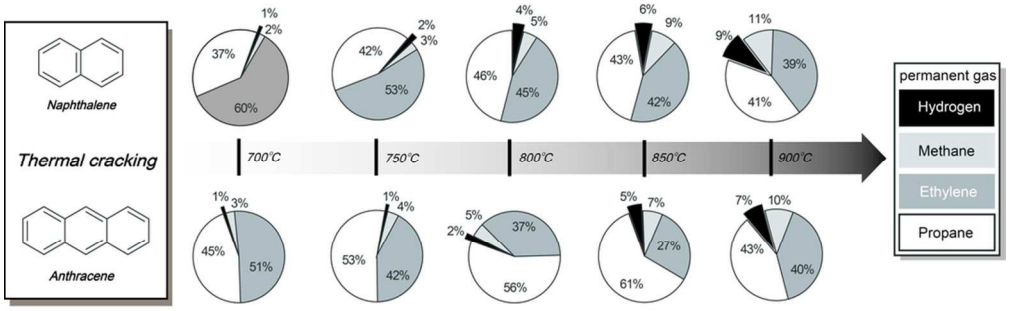

Figure 3 Evolution of gas composition during thermal cracking of naphthalene and anthracene as a function of temperature.

91x29mm (300 x 300 DPI)

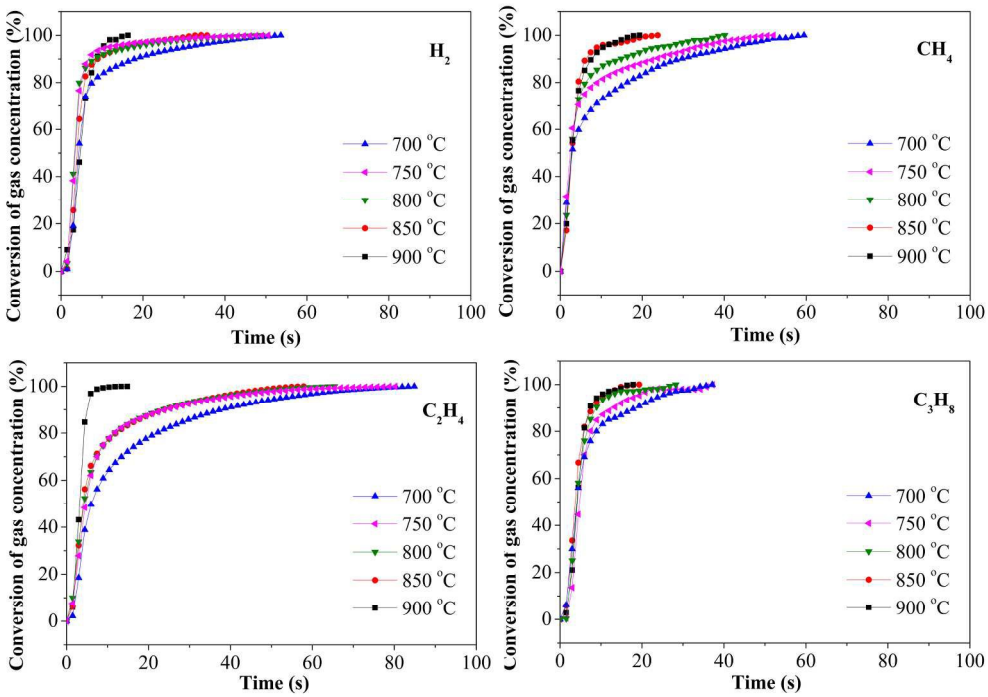

Figure 4 Evolution of conversion fractions versus reaction time at different temperatures for the thermal decmoposition of naphthalene.

210x148mm (300 x 300 DPI)

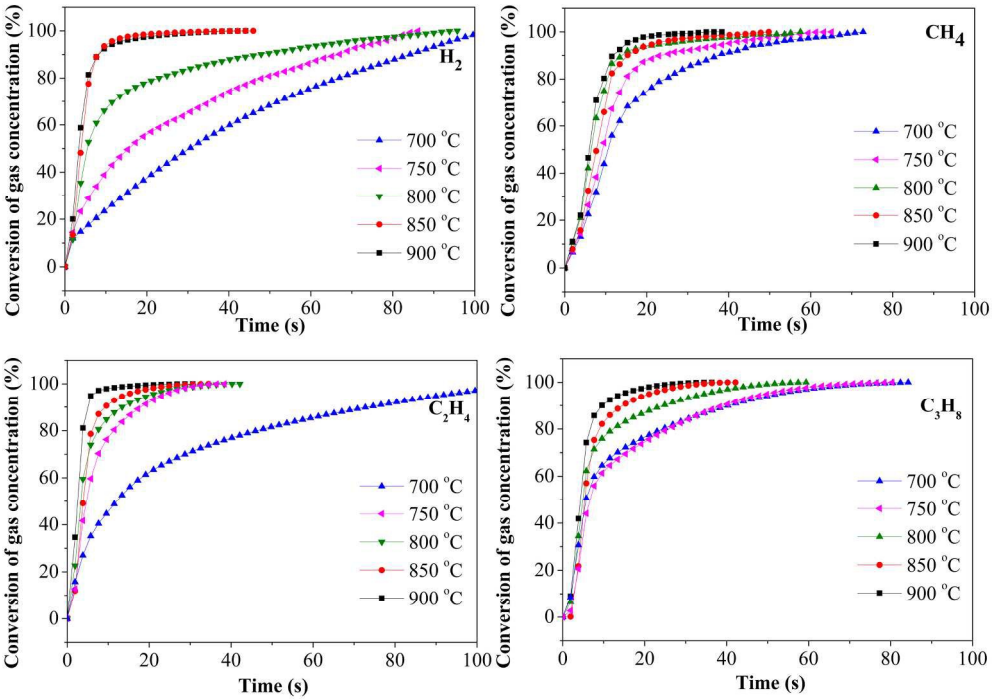

Figure 5 Evolution of conversion fractions versus reaction time at different temperatures for the thermal decomposition of anthracene.

210x148mm (300 x 300 DPI)

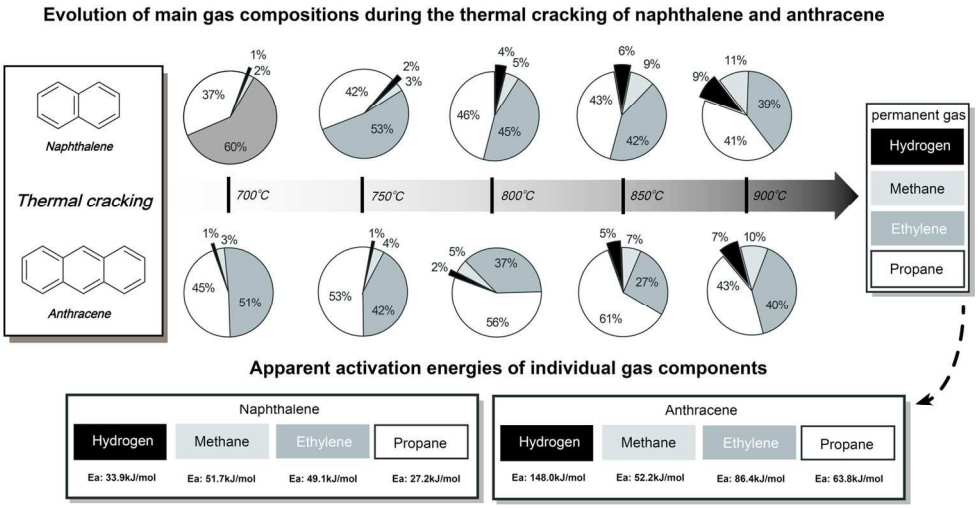

Figure 6 Thermal decomposition behavior and kinetic analysis of naphthalene and anthracene in lab-scale fluidized bed reaction system.

143x71mm (300 x 300 DPI)

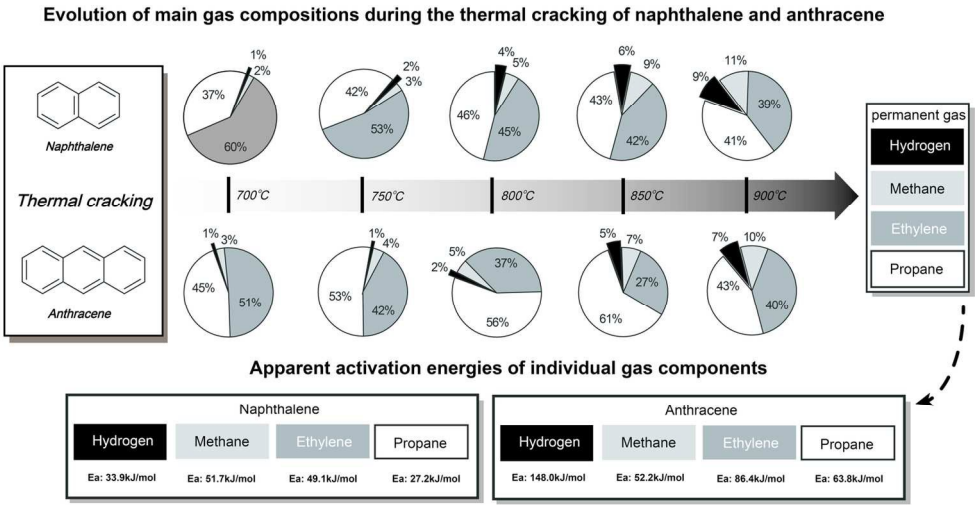

Graphic abstract: Thermal decomposition behavior and kinetic analysis of naphthalene and anthracene in lab-scale fluidized bed reaction system

143x71mm (300 x 300 DPI)